Neuron, Vol. 44, 439–451, October 28, 2004, Copyright ©2004 by Cell Press

Nogo-66 Receptor Prevents Raphespinal and Rubrospinal Axon Regeneration and Limits Functional Recovery from Spinal Cord Injury

Ji-Eun Kim, Betty P. Liu, James H. Park, and Stephen M. Strittmatter*
Departments of Neurology and Neurobiology
Yale University School of Medicine
New Haven, Connecticut 06510

Summary

Axon regeneration after injury to the adult mammalian CNS is limited in part by three inhibitory proteins in CNS myelin: Nogo-A, MAG, and OMgp. All three of these proteins bind to a Nogo-66 receptor (NgR) to inhibit axonal outgrowth in vitro. To explore the necessity of NgR for responses to myelin inhibitors and for restriction of axonal growth in the adult CNS, we generated *ngr*$^{-/-}$ mice. Mice lacking NgR are viable but display hypoactivity and motor impairment. DRG neurons lacking NgR do not bind Nogo-66, and their growth cones are not collapsed by Nogo-66. Recovery of motor function after dorsal hemisection or complete transection of the spinal cord is improved in the *ngr*$^{-/-}$ mice. While corticospinal fibers do not regenerate in mice lacking NgR, regeneration of some raphespinal and rubrospinal fibers does occur. Thus, NgR is partially responsible for limiting the regeneration of certain fiber systems in the adult CNS.

Introduction

The regeneration of axons is profoundly restricted in the central nervous system of adult mammals. Failed axon growth has been ascribed both to glial scar components containing chondroitin sulfate proteoglycans and to the presence of myelin-associated inhibitory molecules. Three protein constituents of oligodendrocytes have been implicated in the inhibitory properties of CNS myelin: Nogo-A, myelin-associated glycoprotein (MAG), and oligodendrocyte-myelin glycoprotein (OMgp) (McGee and Strittmatter, 2003). Nogo-A appears to have two inhibitory domains, an amino terminal domain that acts on many cell types (Amino-Nogo) and an extracellular domain flanked by two hydrophobic segments, termed Nogo-66, that selectively inhibits postnatal axon growth (Fournier et al., 2001b; GrandPre et al., 2000). The Nogo-66 domain binds with high affinity to a GPI-anchored Nogo-66 receptor (NgR) protein found on neuronal membranes (Fournier et al., 2001b). NgR expression can render cells Nogo-66 responsive in vitro. The Amino-Nogo domain functions through unknown NgR-independent mechanisms. The two other myelin-derived axon growth inhibitors, MAG and OMgp, also bind to NgR despite their lack of sequence similarity with Nogo-66 (Domeniconi et al., 2002; Fournier et al., 2001a; Liu et al., 2002; Wang et al., 2002a). Thus, three of the four known axon inhibitors in CNS myelin appear to utilize one receptor system.

*Correspondence: stephen.strittmatter@yale.edu

The relative importance of these myelin inhibitory protein domains has been probed in various experiments in vivo, especially after spinal cord injury (SCI). Antibodies directed against Nogo-A promote regeneration and collateral sprouting from corticospinal (CST) fibers and serotonergic fibers with improved locomotor function after SCI (Bregman et al., 1995). Genetic deletion of Nogo-A allows CST fiber regeneration after SCI to a variable extent in some but not all studies (Kim et al., 2003b; Simonen et al., 2003; Zheng et al., 2003). The basis for this phenotypic variation is not clear but might relate to strain background, specific targeting events, age, or unidentified factors (Woolf, 2003). Mice lacking MAG have not shown CST regeneration after SCI (Bartsch et al., 1995). A peptide derived from Nogo-66 (NEP1-40) functions as a selective antagonist of Nogo-66 stimulation of the NgR but does not antagonize MAG or OMgp action. This peptide, delivered locally or systemically, promotes both CST and raphespinal sprouting even when administered 1 week after SCI (GrandPre et al., 2002; Li and Strittmatter, 2003). The improved locomotion of NEP1-40-treated rodents indicates that Nogo-66 plays a role in limiting regeneration and recovery after injury. Furthermore, a soluble dominant-negative NgR protein pumped intrathecally or overexpressed in transgenic animals is able to promote axonal regeneration and functional recovery following partial SCI (S. Li, B.P.L., and S.M.S., unpublished data).

Despite these studies, a physiologic role for NgR in directly limiting CNS axonal regeneration has not been examined with genetic methods. It is noteworthy that the two proteins most closely related to NgR, namely NgR2 and NgR3, do not bind Nogo-66, MAG, or OMgp in vitro (Barton et al., 2003). Thus, null mutations of the *ngr* gene may be predicted to delineate the role of all three myelin inhibitors separately from Amino-Nogo. Here, we have characterized mice lacking NgR protein and subjected them to SCI. Our findings point to a role for NgR in signaling pathways limiting axonal growth after injury in the adult CNS.

Results

Mice Lacking NgR Are Viable

Embryonic stem cells electroporated with a *ngr*-targeting vector (Figure 1A) were screened using positive (*neo*^{R}) and negative (*hsv-tk*) selection markers. A single clone with the correct homologous recombination pattern was identified by Southern blotting (Figure 1B). A mouse strain established from this clone by blastocyst injection is viable in the homozygous state and selectively disrupts *ngr* expression (Figures 1D and 1E). The expression of *nogo-a* and *nogo-c* mRNA (Figure 1D) and Nogo-A protein (data not shown) is upregulated in postnatal day 6 (P6) brains from *ngr*$^{-/-}$ mice. Immunoblots for Nogo-A in *ngr*$^{-/-}$ adult spinal cord demonstrate persistence upregulation of protein levels (Figures 1F and 1G). The expression of other myelin proteins, including a second NgR ligand, MAG, is not altered in

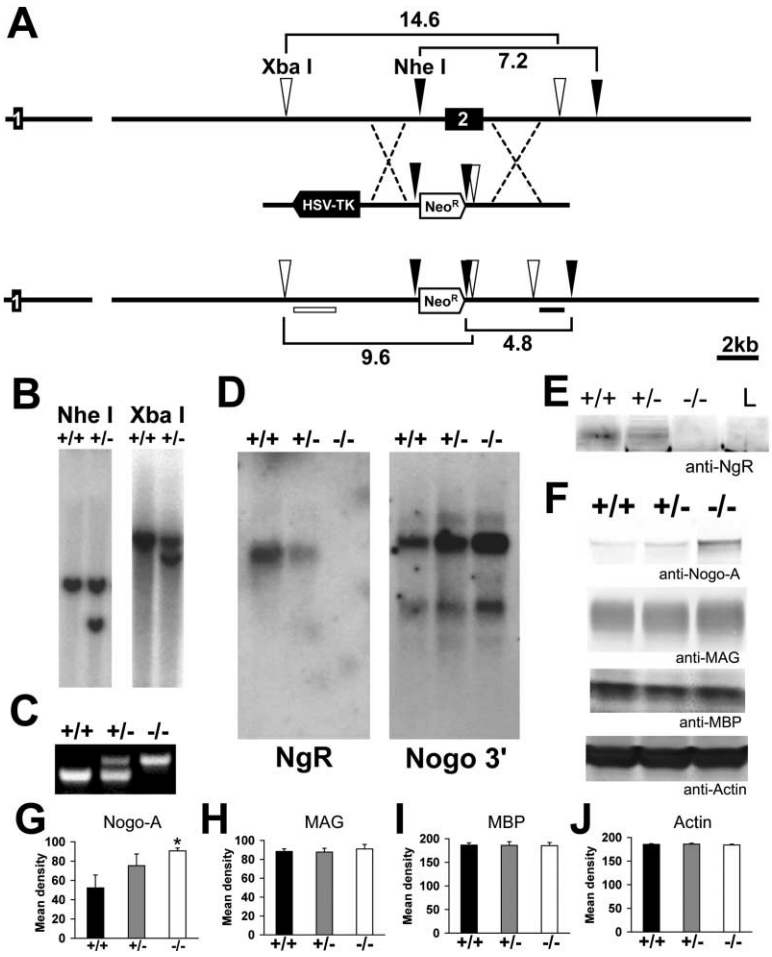

Figure 1. Deletion of Exon 2 of the Mouse *ngr* Gene by Targeted Homologous Recombination

(A) Diagram of the targeting vector and predicted recombination event. A restriction map illustrates the native exons of the mouse *ngr* gene and introduction of new NheI and XbaI restriction sites.

(B) Southern blot analysis of NheI- and XbaI-digested genomic DNA from electroporated ES cells. Hybridization with PCR-amplified probe fragments (shown in [A]) yields a 7.2 or 14.6 kb wild-type band and a shorter 4.8 or 9.6 kb fragment from the disrupted gene after NheI or XbaI digestion, respectively.

(C) Typical genotyping PCR bands using exon 2- and Neo^R-specific primers.

(D) Northern blot analysis of *ngr* mRNA using a *ngr* exon 2 probe and of *nogo* mRNA using a *nogo* 3′ probe in the brains of postnatal day 6 (P6) $ngr^{+/+}$, $ngr^{+/-}$, and $ngr^{-/-}$ mice.

(E) Western blot analysis for NgR protein expression in adult brain lysates of $ngr^{+/+}$, $ngr^{+/-}$, and $ngr^{-/-}$ mice. Liver lysate (L) is included as a negative control.

(F) Western blot analysis for Nogo-A, MAG, MBP, and Actin protein expression in adult spinal cord lysates of $ngr^{+/+}$, $ngr^{+/-}$, and $ngr^{-/-}$ mice.

(G–J) Densitometric analysis of spinal cord protein levels determined from immunoblots as in (F). Values are means ± SEM from five separate animals of each genotype. *Significantly different from wild-type, $p < 0.05$ (Student's t test).

$ngr^{-/-}$ spinal cord (Figures 1F, 1H, and 1I). The adult brain does not exhibit persistent Nogo-A upregulation (data not shown), possibly because the brain contains relatively more gray matter than does spinal cord and increased oligodendrocyte expression is masked by unaltered neuronal expression. The mRNA level for *nogo-b* in the adult brain is normally very low, and its level is not significantly altered in this strain of mice.

Mice from the $ngr^{-/-}$ line are born at expected Mendelian frequencies and grow with normal body weights. Both males and females are fertile. No unexpected deaths have been witnessed in homozygous animals up to 13 months of age.

Normal Brain Histology and Behavior in NgR Null Mice

NgR expression is neuron specific and widespread in the adult CNS (Wang et al., 2002b). NgR interaction with the myelin-associated proteins Nogo, MAG, and OMgp raises the possibility that NgR is necessary for maintaining myelin/axon structure (Wang et al., 2002b; Huber et al., 2002). However, brain size and gross anatomy are normal in adult $ngr^{-/-}$ mice; there are no gross abnormalities in the white matter tracts of the brain and spinal cord as assessed by Luxol fast blue staining for total myelin content and location (Figures 2C and 2D). Major brain nuclei and the neuronal layers of the cerebral cortex and cerebellum are indistinguishable from those of wild-type mice by hematoxylin and eosin staining (Figures 2A and 2B). The data indicate that neuronal placement and survival is normal in adult $ngr^{-/-}$ mice.

Despite the normal appearance of these histologic parameters, the absence of NgR might change neuronal function and mouse behavior through effects on axonal performance. Quantitative neurological examination of the mice lacking NgR does reveal deficits in function. Open field behavioral parameters are distinct from wild-type littermates (Figures 2E and 2F). The knockout mice spend more time in the marginal zone of an open field activity monitoring enclosure and make fewer movements during the 15 min period, suggesting increased anxiety levels when placed in a novel environment. The rotarod test was employed to assess motor coordination and learning. $ngr^{-/-}$ mice performed worse than wild-type or heterozygous littermates on the rotarod (Figure 2G). The Basso-Beattie-Bresnahan (BBB) score is another measure of locomotor function in the open field and is commonly used to assess deficits after SCI (Basso et al., 1996; Joshi and Fehlings, 2002). Despite the subnormal performance on the rotarod, uninjured $ngr^{-/-}$ mice exhibit a full range score, similar to controls (Figures 4A and 4B). Overall, routine anatomical and

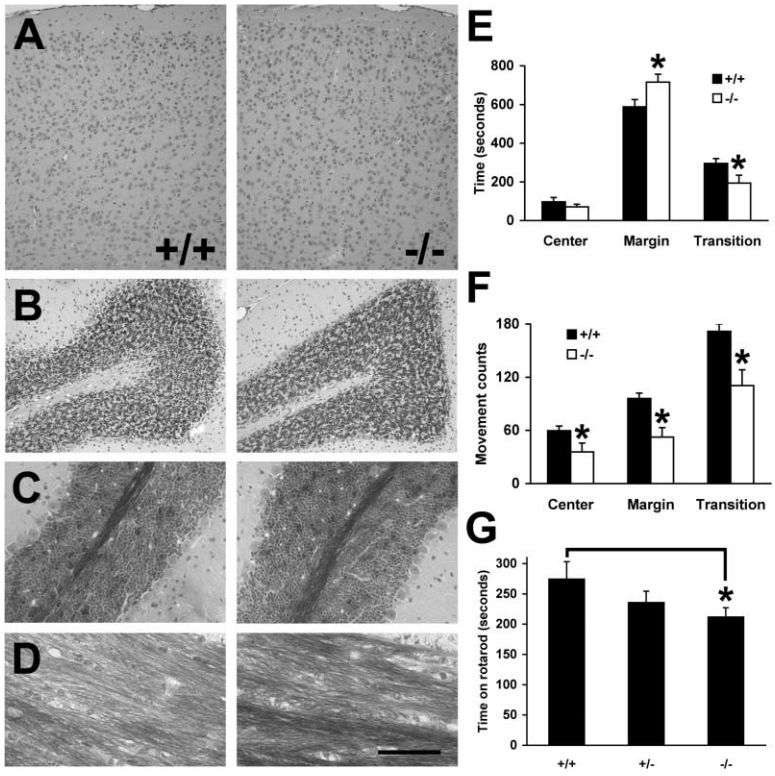

Figure 2. General Brain Histology and Locomotor Activity in $ngr^{+/+}$ and $ngr^{-/-}$ Mice

(A) Coronal sections through the cerebral cortex stained with hematoxylin and eosin. (B and C) Parasagittal sections through the cerebellum stained with hematoxylin and eosin (B) or Luxol fast blue (C). (D) Corpus callosum in coronal sections stained with Luxol fast blue. Scale bar indicates 200 μm (A and B), 100 μm (C), or 50 μm (D). (E and F) Open field activity. Floor plane sensor measurements collected from an automated activity monitoring cage for $ngr^{+/+}$ and $ngr^{-/-}$ mice are graphed according to time spent (E) and movement counts (F) in three arbitrarily designated zones. (G) Rotarod test. The time that mice were able to remain on the rotating rod at constantly accelerating speeds is reported. All data are represented as mean ± SEM. *Significantly different from wild-type, $p < 0.05$ (Student's t test).

locomotor analysis demonstrates significant but nonlethal deficits in the NgR null mice.

Neurons Lacking NgR Are Less Sensitive to Nogo-66

If NgR is the only receptor for Nogo-66, then ligand binding and biological responses will be absent from $ngr^{-/-}$ neurons. Wild-type DRG neurons bind AP-Nogo-66, but neurons from $ngr^{-/-}$ mice do not do so significantly above background levels (Figures 3A and 3B). The absence of high-affinity binding sites for Nogo-66 in *ngr* null cells predicts that Nogo-66 will not inhibit their axonal growth properties. A series of myelin inhibitory proteins were examined for growth cone collapsing activity in wild-type versus $ngr^{-/-}$ P14 DRG cultures. Nogo-66, MAG, OMgp, and CNS myelin all fail to induce growth cone collapse in postnatal DRG neurons lacking NgR (Figures 3C and 3D).

Improved Locomotor Recovery after SCI in $ngr^{-/-}$ Mice

Since postnatal DRG neurons lacking NgR appear significantly less sensitive to myelin inhibitors in vitro, the degree of recovery from SCI in vivo was assessed. Locomotor recovery from a midthoracic dorsal hemisection injury was assessed using a standardized open field assessment, the BBB score (Figure 4A). All mice had scores of 0 to 3 at 4 hr postinjury (data not shown). The $ngr^{+/+}$ and $ngr^{+/-}$ mice gradually recover partial function over a 21 day observation period. The BBB scores of $ngr^{-/-}$ mice are significantly higher than controls throughout the 2–21 day period, especially in the third week post-SCI. The improved scores of the $ngr^{-/-}$ mice are comparable to those observed in one line of *nogo-a/b* knockout mice (Kim et al., 2003b).

Because recovery from dorsal hemisection injury is quite pronounced even in wild-type mice, a more stringent test of post-SCI regeneration was examined by creating a complete spinal cord transection at thoracic level 8 (T8; Figures 4B and 4C). The completeness of such lesions is obvious from GFAP immunohistology of parasagittal sections (Figure 4C). Rostral and caudal astroglial scars surround a central fibroblastic, GFAP-negative scar in all sections examined (Figure 4C). There is no evidence of any spared tissue bridges in eight of eight $ngr^{-/-}$ and four of four $ngr^{+/-}$ mice examined by GFAP immunostaining. The *ngr* null mice display significantly higher locomotor scores during the weeks after complete transection injury than do control littermates (Figure 4B). At 6 weeks post-SCI, the control mice recover to an average score of 7. Others have recently reported significant treadmill-induced locomotion in mice with complete spinal transection, so this level of improvement in wild-type and $ngr^{+/-}$ mice should not be unexpected (Leblond et al., 2003). Mice lacking NgR recover to significantly higher scores than do control mice, with a majority of the $ngr^{-/-}$ mice reaching a score of 9 or greater by 6 weeks (Figure 4B). These open field scores at 6 weeks reflect a highly significant increase (Student's t test; $p \leq 0.001$) in the achievement of weight-bearing postures from a rarity in control mice to over 80% of $ngr^{-/-}$ mice (Figures 4B and 4H–4J). Given the poorer rotarod performance and reduced activity of the $ngr^{-/-}$ animals prior to injury (Figure 2), their improved function postinjury is all the more remarkable.

Functional improvement in the complete spinal transected mice might be attributed either to alterations in

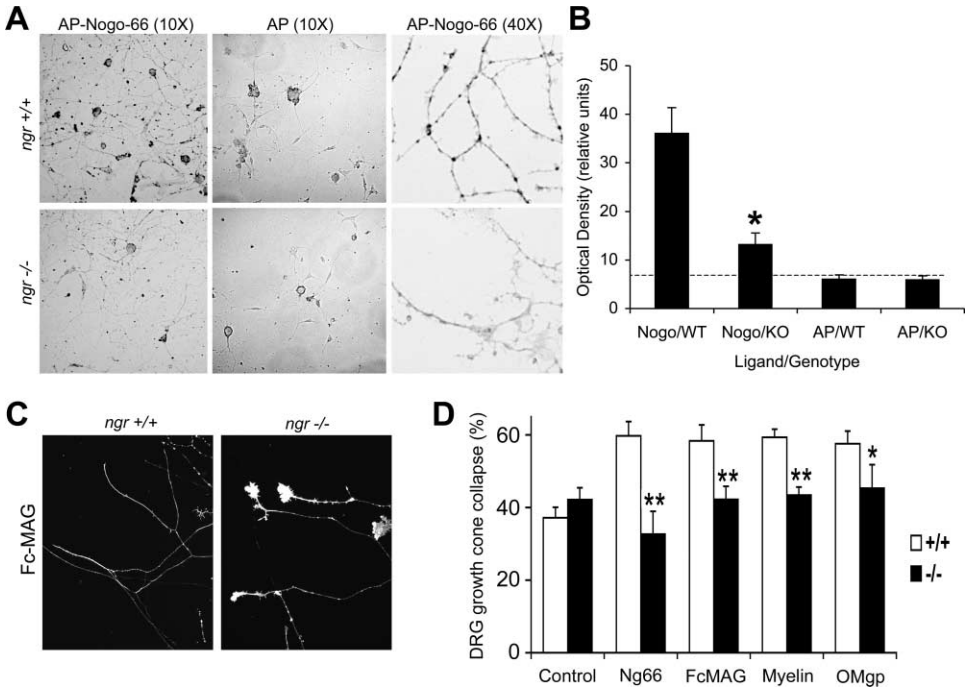

Figure 3. Neurons Lacking NgR Do Not Bind Nogo-66 and Are Not Inhibited by Nogo-66

(A) AP-Nogo-66 or AP binding (50 nM) to dissociated P6 DRG neurons from $ngr^{+/+}$ or $ngr^{-/-}$ mice. Higher magnification of the selective staining of neurites by AP-Nogo-66 in the wild-type mice is shown at the right. (B) Quantitation of AP bound to neurons cultured as in (A). (C) Growth cone morphology after exposure of $ngr^{+/+}$ or $ngr^{-/-}$ P14 DRG axons to MAG-Fc protein, as revealed by rhodamine-phalloidin. (D) The percentage of collapsed growth cones from cultures as in (C) was measured after exposure to GST-Nogo-66 (100 nM), MAG-Fc (100 nM), CNS myelin (1.6 μg protein/ml), or OMgp (50 nM). All data are represented as mean ± SEM. *Significantly different from wild-type, $p < 0.05$; **$p < 0.01$ (Student's t test).

distal spinal cord intrinsic circuits, such as the locomotor pattern generator, or to the reestablishment of descending pathways that had been severed. To assess descending pathways from the forebrain to the hindlimb motoneuron pool, transcranial magnetic motor-evoked potentials (tcmMEPs) were monitored in the gastrocnemius muscle (Figures 4D–4F). In uninjured mice, the tcmMEP is easily detected with an amplitude of ~700 μV and a latency of 2–2.5 ms. Six weeks after complete transection injury, only 1 of 19 control mice had a response greater than 35 μV. The lesion site of the one animal with a weak response could not be examined by GFAP histology, so it is possible that trace tissue sparing was present, even though the vast majority of animals underwent complete transections (Figure 4C). In stark contrast, 16 of 19 of the $ngr^{-/-}$ mice undergoing the same lesion exhibit a clearly detectable tcmMEP (Figure 4D), including the five $ngr^{-/-}$ mice with histologically verified complete transections as shown in Figure 4C. As expected from a partially reconstituted pathway in the transected $ngr^{-/-}$ mice, the latency of the tcmMEP response is prolonged, and the amplitude is decreased compared to uninjured animals (Figures 4E and 4G). This is not related to altered stimulation or recording efficiency in the $ngr^{-/-}$ mice, since forelimb tcmMEPs were unaffected by the SCI and were of equal amplitude in control and $ngr^{-/-}$ mice (Figure 4F). Thus, reestablishment of descending connections is likely to contribute to the weight-bearing status achieved by a majority of the mice lacking NgR after the more severe spinal lesion.

Lack of Long-Distance Corticospinal Regeneration in the $ngr^{-/-}$ Mice

We sought to ascertain the anatomical basis for the improved locomotor and electrophysiologic recovery observed in the $ngr^{-/-}$ after SCI. In one particular strain of spinal injured *nogo-a/b*$^{-/-}$ mice, the CST system exhibits axonal sprouting and long-distance regeneration in a majority of dorsal-hemisected mice (Kim et al., 2003b). In contrast, anterograde BDA tracing of the injured $ngr^{-/-}$ mice fails to exhibit any CST axon sprouting or long-distance CST regeneration after a dorsal hemisection (Figures 5A and 5B) or after a complete transection (data not shown). No ectopic CST sprouts ipsilateral to the BDA injection and rostral to the lesion were observed in the $ngr^{-/-}$ mice. Of 12 hemisected $ngr^{-/-}$ mice examined, only two mice showed BDA-labeled fibers caudal to the lesion site, but the number of such fibers was much lower (two to four fibers per section) than in the strain of *nogo-a/b* null mice with significant fiber growth (Kim et al., 2003b). Despite the fact that this labeling technique detects only a small fraction (1%) of all CST fibers, it seems doubtful that the CST fiber system accounts for the behavioral or electrophysiologic recovery. The CST phenotype of the spinal injured $ngr^{-/-}$ mice matches that of the *nogo-a/b*$^{-/-}$ mice lacking CST regeneration

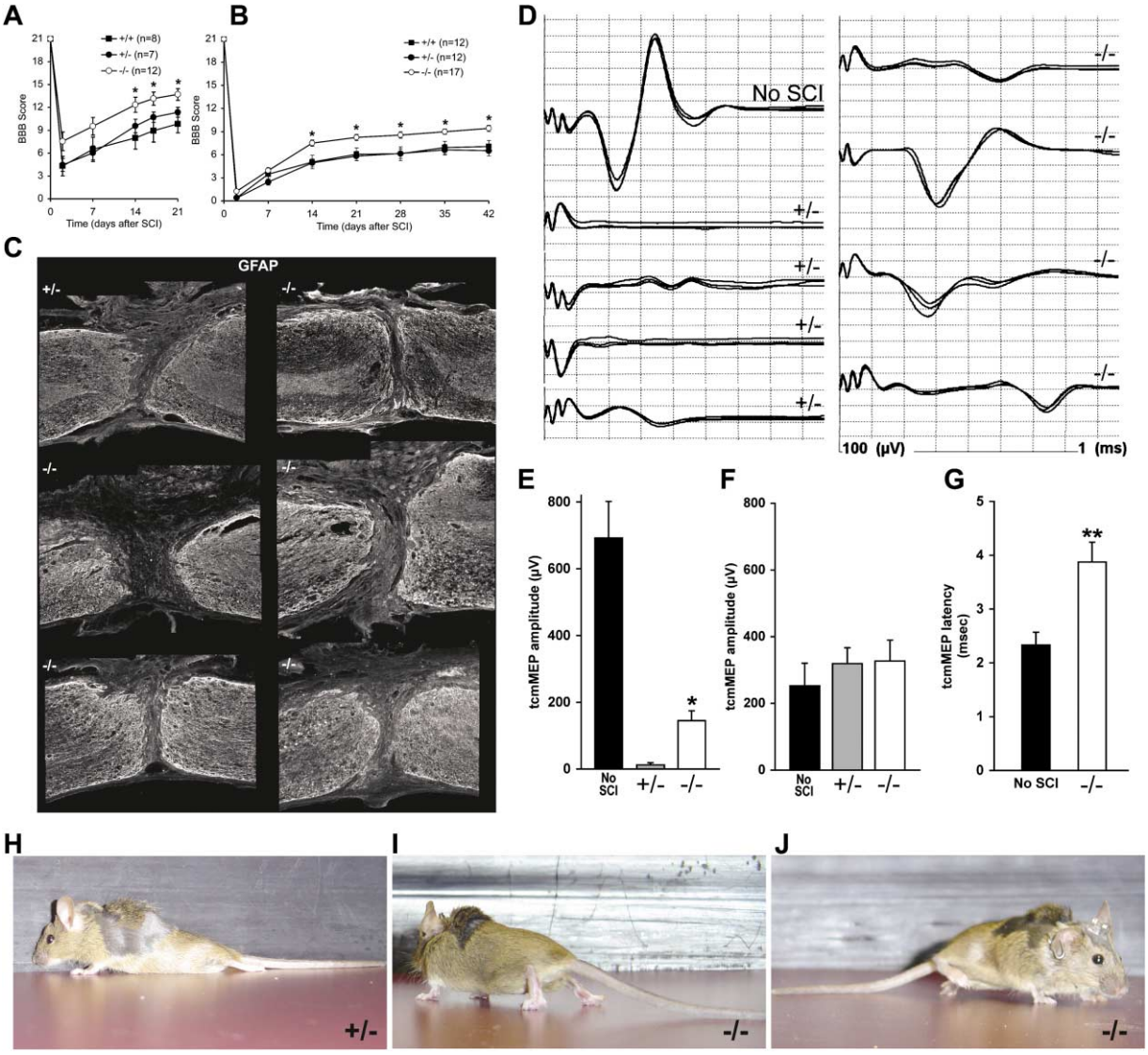

Figure 4. Improvement of Locomotor Scores in NgR Knockout Mice after Dorsal Hemisection or Complete Transection of the Spinal Cord

(A and B) Comparison of open field locomotor activity in $ngr^{+/+}$, $ngr^{+/-}$, or $ngr^{-/-}$ mice following dorsal hemisection (A) or complete transection (B) of the spinal cord. (C) Anti-GFAP histology of parasagittal sections across the injury site from individual complete transection animals of the indicated genotypes demonstrates the complete nature of the lesions. Rostral is to the right and dorsal is up in this and all parasagittal sections. (D) Representative gastrocnemius tcmMEP from separate uninjured mice, complete transection $ngr^{+/-}$ mice, and complete transection $ngr^{-/-}$ mice. Studies of the injured mice were performed 6 weeks posttransection. The transcranial magnetic stimulus was applied at time zero. Each horizontal tick represents 1 ms, and each vertical tick corresponds to 100 μV. Three separate stimuli administered to each animal are superimposed. (E) The average amplitude of the gastrocnemius tcmMEP from experiments as in (D) is represented. The 14 of 19 $ngr^{+/-}$ mice with no significant response and the 3 of 19 $ngr^{-/-}$ mice with no response are included in the averages. (F) The average amplitude of the forelimb biceps tcmMEP is represented. The $ngr^{+/-}$ (n = 9) and $ngr^{-/-}$ (n = 5) mice were recorded 6 weeks after a complete thoracic spinal transection. (G) The average tcmMEP response latencies for uninjured and $ngr^{-/-}$ mice. All data are represented as mean ± SEM. *Significantly different from wild-type, $p \leq 0.005$; **$p < 0.05$ (Student's t test). (H) Photograph of a $ngr^{+/-}$ mouse 6 weeks after complete thoracic SCI demonstrating inability to support weight with hindlimbs. (I and J) Examples of a $ngr^{-/-}$ mouse at 6 weeks post-complete SCI reveals weight support (I and J) and stepping (J) with the hindlimbs.

(Zheng et al., 2003) but differs from that of the *nogo-a/b*$^{-/-}$ strain with detectable CST growth (Kim et al., 2003b).

Rubrospinal Axon Regeneration after SCI in *ngr*$^{-/-}$ Mice

Since CST fibers do not regenerate to any great extent across the spinal injury site, we considered other neuronal populations. Successful axonal regeneration is associated with the induction of a number of proteins in the neuron. SPRR1A is one marker of productive peripheral regeneration that contributes directly to axonal extension (Bonilla et al., 2002; Kim et al., 2003a). Examination of transverse sections above and below the lesion site demonstrates a significant increase in SPRR1A-positive fibers and cell bodies in the $ngr^{-/-}$ mice (Figures 5C–5E).

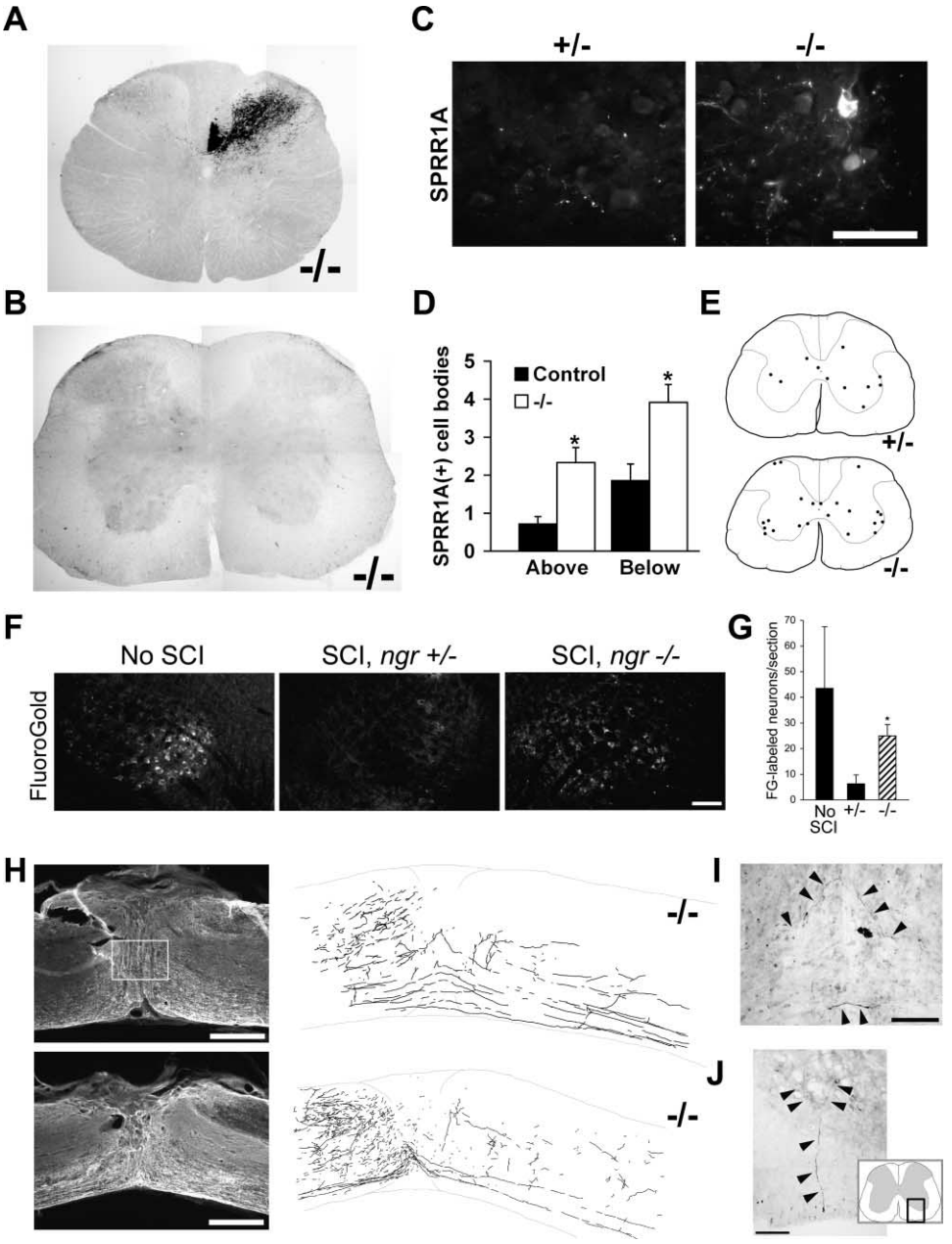

Figure 5. Rubrospinal Axon Growth in $ngr^{-/-}$ Mice after Complete Transection

(A and B) Lack of CST axon sprouting and regeneration in NgR null mice following dorsal hemisection of the spinal cord. Cross-sections of spinal cord from a representative $ngr^{-/-}$ mouse, 21 days postinjury, 5 mm rostral (A) or 5 mm caudal (B) to the transection. The BDA-injected cerebral cortex corresponds to the left of these sections, so the majority of crossed dCST fibers are on the right. No fibers are detected below the lesion. (C) Cross-sections of spinal cord 5 mm caudal to the lesion from $ngr^{+/-}$ and $ngr^{-/-}$ mice, 6 weeks post-SCI, stained with anti-SPRR1A antibody. Scale bar, 100 μm. (D) Quantitation of total SPRR1A-positive cell bodies per transverse section throughout the spinal gray matter area found in control and $ngr^{-/-}$ mice, 5 mm rostral or 5 mm caudal to lesion. (E) Schematic summarizing the location of SPRR1A immunoreactive cells in the lumbar spinal cord of $ngr^{+/-}$ and $ngr^{-/-}$ mice, 6 weeks post-SCI. The cell location from one section of each of five animals is plotted on one schematic. (F) Coronal section of the red nucleus after Fluorogold injection into the lumbar ventral horn of uninjured mice, complete transection $ngr^{+/-}$ mice, and complete transection $ngr^{-/-}$ mice. Scale bar, 100 μm. (G) The average number of retrogradely labeled rubrospinal neurons per transverse section at the level of the magnocellular red nucleus as in (D). (H) Anterograde tracing of the rubrospinal tract. BDA was injected into the red nucleus bilaterally 6 weeks after a complete transection of the thoracic spinal cord. Anti-GFAP staining of longitudinal sections of the spinal cord demonstrates the lesion site (right panels) and camera lucida drawings from two separate $ngr^{-/-}$ mice demonstrating the course of BDA-labeled fibers in all parasagittal sections at the same level (left panels). Scale bar, 400 μm. (I) Rubrospinal fibers crossing the lesion site of $ngr^{-/-}$ mice. BDA staining of the region boxed in (H) is illustrated at higher magnification. Scale bar, 100 μm. (J) Transverse section of lumbar spinal cord from a $ngr^{-/-}$ mouse illustrating a BDA-positive rubrospinal fiber in the lumbar spinal cord after complete spinal transection. The schematic illustrates the location of the micrograph. Scale bar, 100 μm. All data are represented as mean ± SEM. *Significantly different from wild-type, $p < 0.05$ (Student's t test). Scale bar, 400 μm.

The appearance and location of the SPRR1A-positive cell bodies in the spinal gray matter of the injured *ngr*$^{-/-}$ mice are consistent with spinal interneurons. This may reflect an increased propensity for plastic rearrangements of intrinsic spinal circuitry in this strain. SPRR1A-positive cell bodies were not identified in the cerebral cortex or the brainstem of the same animals (data not shown).

In order to reveal which, if any, particular descending tracts might contribute to electrophysiologic and behavioral recovery, we performed retrograde tracing with Fluorogold (FG) from the caudal ventral horn of completely transected mice 6 weeks after injury. Control animals reveal no significant label in the brainstem, as expected. However, in the *ngr*$^{-/-}$ samples, there are significant numbers of FG-positive neurons in the red nucleus (Figures 5F and 5G). The absolute density of labeled rubrospinal neurons in the *ngr*$^{-/-}$ mice 6 weeks after complete transection injury reaches forty percent of the value obtained in uninjured mice (Figures 5F and 5G). A few FG-positive neurons are also detected in the medullary reticular formation, the pontine nuclei, the vestibular nuclei, and the raphe of the *ngr*$^{-/-}$ mice (data not shown). All of these retrogradely labeled structures are thought to contribute to locomotion and together provide a significant regenerated descending input to the lumbar spinal cord after complete transection in the *ngr*$^{-/-}$ mice. As expected from the BDA tracing, no FG-positive neurons are detected in the cerebral cortex (data not shown).

To investigate the rubrospinal system more directly, anterograde tracing studies were conducted after complete transection of the thoracic spinal cord. In three of six injured *ngr*$^{-/-}$ mice, but in none of eight *ngr*$^{+/-}$ mice, rubrospinal fibers crossing the lesion site were detected (Figures 5H and 5I), and some fibers reached the lumbar spinal cord (Figure 5J). Thus, a limited degree of rubrospinal regeneration occurs in the absence of NgR.

Raphespinal Fibers Regenerate in the Absence of NgR

The serotonergic raphespinal system contributes to locomotor circuitry and can be assessed in an anterograde fashion by simple immunohistology, since it is the only source of serotonergic input to the adult spinal cord. Furthermore, the raphespinal tract is one of the tracts shown to have enhanced regeneration following NgR antagonist treatment studies (GrandPre et al., 2002; Li and Strittmatter, 2003). In control *ngr*$^{+/-}$ mice with complete transections, it is notable that 5-HT fibers are present throughout the rostral astrocytic scar and do not retract from the lesion site as do CST fibers (Figure 6A). As an additional step to consider the potential responsiveness of serotonergic systems to *ngr* gene disruption, we assessed whether this population expresses NgR protein in wild-type animals. Indeed, double label immunohistology demonstrates that serotonergic neurons in the brainstem raphe do express NgR (Figure 6B).

After complete transection injury, no 5-HT immunoreactive fibers are observed extending through the injury site into caudal tissue from parasagittal sections of five of five control *ngr*$^{+/-}$ mice. The pattern in *ngr*$^{-/-}$ complete-transected spinal tissue is very different, with a subset of fibers crossing into spinal tissue caudal to the injury site (Figure 6C). In GFAP/5-HT double immunohistology, serotonin-positive fibers are detectable beyond the astrocytic scar and are observed to extend into the fibroblastic scar area (Figures 6D–6F). High magnifications of all serial sections from one *ngr*$^{-/-}$ animal allowed a camera lucida reconstruction of the pattern of caudal growth beyond the injury site (Figures 6G and 6H). Cross-sections of the spinal cord at a level 4 mm caudal to the complete transection were also examined for 5-HT-positive profiles (Figures 7A and 7D). In completely transected spinal cords, the level of serotonergic fiber length per section at this level is essentially undetectable in control mice. In *ngr*$^{-/-}$ mice, regenerated serotonergic fibers are evident in the majority of the complete transected animals (Figures 7A and 7D). Thus, the presence of NgR in raphespinal axons of wild-type mice is at least one of the factors limiting their regeneration after transection in the adult spinal cord.

In those mice with dorsally hemisected spinal cords, a significant proportion of raphespinal fibers are spared in the distal cord following injury. Therefore, we conducted a parallel analysis of the raphespinal system in this experiment that concentrated on the two areas that had the highest density of innervation, the intermediolateral cell column and ventral horn. Quantitation of 5-HT-positive fiber length in a defined area of these two regions indicates a significantly higher innervation density in the *ngr*$^{-/-}$ mice compared to wild-type littermates (Figures 7B and 7C). The return of caudal 5-HT fiber density closer to control values may reflect local sprouting of collaterals and could account for the early (2 day postinjury) behavioral improvement of the *ngr*$^{-/-}$ mice after dorsal hemisection (Figure 4A).

Raphespinal Tract Contributes to Functional Recovery in *ngr*$^{-/-}$ Mice

Since a marked degree of raphespinal tract regeneration occurs in the *ngr*$^{-/-}$ mice, we sought to assess the importance of this fiber system for the observed improvement in functional recovery. A serotonergic neurotoxin, 5,7-dihydroxytryptamine (5,7-DHT) was injected intracerebroventricularly (i.c.v.) to kill raphe nucleus neurons and deplete serotonergic inputs to the lumbar spinal cord (Figure 7E). 5,7-DHT was administered at 4 weeks post-SCI, when the difference in BBB scores between heterozygote and knockout littermates was established. BBB scores were assessed 2, 7, and 10 days after 5,7-DHT injection. While the BBB score continued to gradually improve in the heterozygotes, scores started to decline in the knockouts, becoming indistinguishable from the heterozygotes by 10 days (Figure 7E). These results strongly suggest that the improvement of weight-bearing postures in the knockout mice is mediated at least in part by recovery of raphespinal inputs caudal to the lesion.

Discussion

The hypothesis that NgR contributes to the limitation of adult CNS regenerative growth is demonstrated by several major findings from this study of mice lacking NgR. First, DRG axonal growth cones lacking NgR are

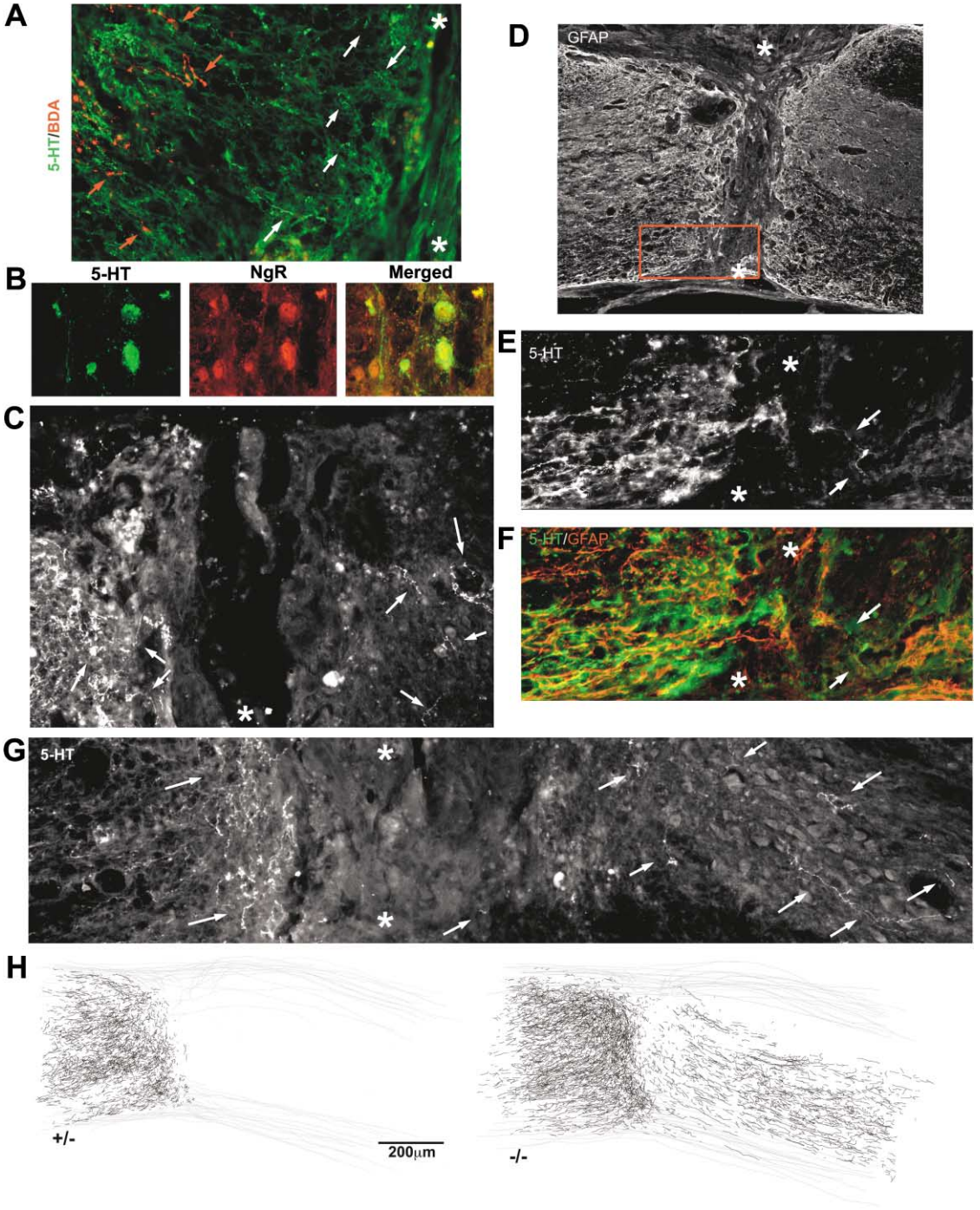

Figure 6. 5-HT Fiber Regeneration after Complete Spinal Transection in Mice Lacking NgR

(A) Parasagittal section from a complete transected control $ngr^{+/-}$ mouse stained to reveal both CST (BDA, red) and raphespinal (5-HT, green) fibers. Note that 5-HT fibers are present more caudally than are CST fibers, but not at the center of the lesion marked with asterisks.

(B) Neurons double stained for 5-HT and NgR in the raphe nucleus of the brainstem.

(C) An anti-serotonin antibody-stained parasagittal section across a complete transection site from a $ngr^{-/-}$ mouse demonstrates regenerating raphespinal fibers (arrows) caudal to the fibroblastic scar (marked by the asterisks).

(D) Low-magnification view of a GFAP-stained parasagittal section from a complete transection site from a $ngr^{-/-}$ mouse different from that in (C). The region shown at higher power in (E) and (F) is boxed in red.

(E) Serotonergic immunohistology from the section shown in (D) revealing fine raphespinal fibers (arrows) extending into the region of the GFAP-negative fibroblastic scar.

(F) Double immunohistology of the region in (E) revealing both serotonin (green) and GFAP (red).

(G) Serotonin immunohistology of a parasagittal section from the complete transection site of a different mouse than in (C)–(F) reveals serotonin fibers (arrows) caudal to the injury site (asterisks).

(H) Camera lucida drawing assembled by superimposing multiple high-magnification views of all serial parasagittal sections from one $ngr^{-/-}$ animal, as in (G), and one $ngr^{+/-}$ mouse. The outline of the spinal cord is traced in thin gray, and the 5HT fibers are traced in thick black.

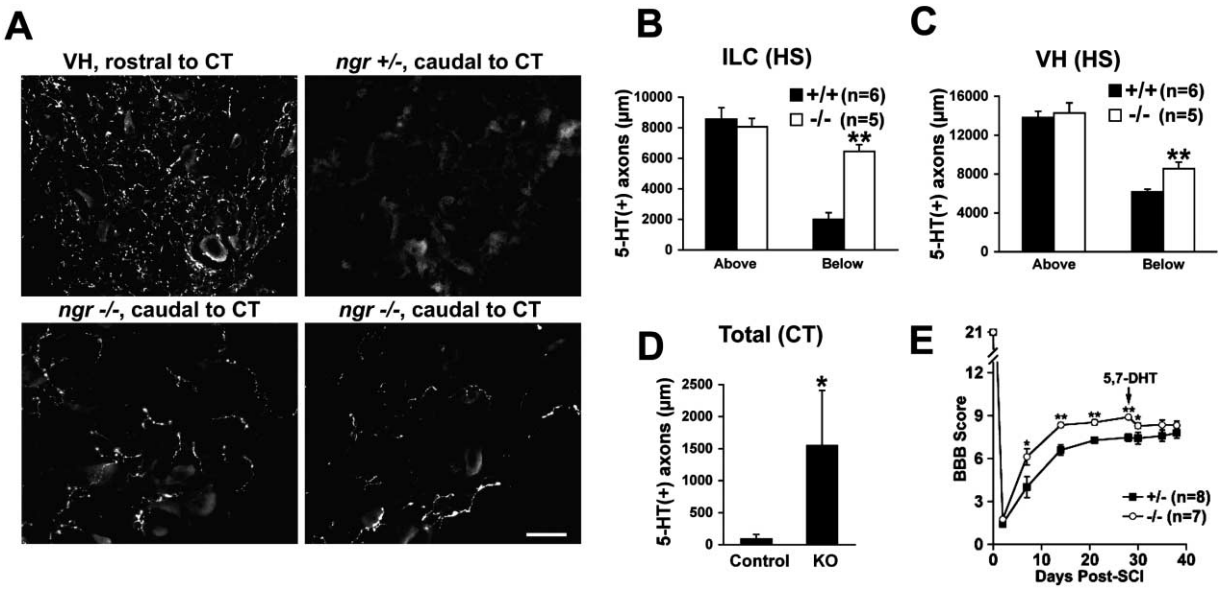

Figure 7. 5-HT Fiber Regeneration into the Caudal Spinal Cord in $ngr^{-/-}$ Mice Contributes to Enhanced Functional Recovery

(A) Cross-sections of spinal cord stained with anti-serotonin antibodies from $ngr^{+/-}$ and $ngr^{-/-}$ mice after complete transection of the spinal cord at a level 4 mm rostral or caudal to the injury site. Scale bar, 50 μm. (B and C) Quantitation of 5-HT-positive fiber length per 35,000 μm^2 found above and below the level of injury in the intermediolateral cell column (ILC) and ventral horn (VH) from $ngr^{+/+}$ and $ngr^{-/-}$ mice after dorsal hemisection (HS). (D) Quantitation of 5-HT-positive fiber length per section found in caudal white and gray matter from $ngr^{+/+}$ and $ngr^{-/-}$ mice after complete transection (CT). (E) Comparison of open field locomotor activity in $ngr^{+/+}$ and $ngr^{-/-}$ mice. 5,7-DHT was i.c.v. injected at 4 weeks post-SCI. All data are represented as mean ± SEM. *Significantly different from wild-type, $p < 0.05$; **$p \leq 0.005$ (Student's t test).

not collapsed by myelin inhibitors in vitro. Second, behavioral and electrophysiologic measures demonstrate significantly enhanced recovery after spinal cord injury. Third, regenerative growth of brainstem neuronal populations into the distal spinal cord occurs in $ngr^{-/-}$ mice. However, not all fiber systems regenerate in the adult spinal cord when NgR is absent. Notably, the CST does not regenerate in $ngr^{-/-}$ mice after spinal cord injury despite its capacity to regenerate in some strains of mice lacking Nogo-A and in mice treated with NgR antagonists (GrandPre et al., 2002; Kim et al., 2003b). We conclude that NgR is one of several factors preventing significant regenerative axon growth of certain fiber systems after CNS axotomy in adult mice.

Neuronal Responses to Myelin Inhibitors Require NgR

Of the four protein domains recognized as myelin-derived inhibitors of axonal outgrowth, three are known to bind to NgR (McGee and Strittmatter, 2003). Since $ngr^{-/-}$ DRG growth cones do not collapse in the presence of Nogo-66, MAG, or OMgp in vitro, we conclude that NgR is required for axon growth inhibition by these proteins, at least in DRG neurons. If other receptors mediate the acute effects of these ligands, they do not appear to be functional in the absence of NgR during DRG culture. It remains possible that other neuronal populations utilize other receptor systems. For example, CST neurons do not regenerate after SCI in the absence of NgR and might utilize such unidentified alternate receptor systems. In contrast to Nogo-66, MAG, and OMgp, the Amino-Nogo domain remains inhibitory for DRG axons in the absence of NgR, confirming that Amino-Nogo does not utilize NgR for axon inhibition.

Homologs of NgR have been identified in both the human and mouse genomes. NgR2/NgRH1 and NgR3/NgRH2 share significant sequence similarity with NgR. Since COS-7 cells transfected with either NgR2 or NgR3 do not bind to any of the known ligands of NgR, these proteins do not appear to be alternate receptors for the myelin inhibitors (Barton et al., 2003). Given that DRG neurons express these NgR homologs (Lauren et al., 2003), the absence of growth cone responses in $ngr^{-/-}$ DRG neurons confirms the selective role of NgR in myelin inhibitory signaling.

Anatomical Regeneration by Selective Subsets of Axons

After SCI, there is anatomical evidence of significant axon regeneration in the $ngr^{-/-}$ mice that is not observed in control animals. A regeneration-associated gene normally induced by axotomy in peripheral neurons, SPRR1A, is expressed in some spinal interneurons of mice lacking NgR. This implies that NgR might possibly contribute to the suppression of those genes that contribute to an enhanced axonal growth state and to modifications of intrinsic circuits in the spinal cord.

Corticospinal tracing experiments indicate that few if any $ngr^{-/-}$ CST axons cross a complete transection injury. However, retrograde and anterograde tracing reveals that axons from several brainstem areas that participate in locomotion do cross these transections. Amongst the regenerating fiber systems are rubrospinal and raphespinal fibers. The basis for the selective

growth of some fibers but not others will require further investigation. It does not seem to be due simply to selective NgR expression, since NgR is expressed strongly both in brainstem nuclei and in the pyramidal cells of the cerebral motor cortex. It may be that regenerating fiber systems such as the raphespinal tract are more prone to plastic changes in the adult than is a more static CST system. However, even in the absence of NgR, brainstem neurons do not express SPRR1A in response to spinal injury. Thus, this axonal growth marker alone cannot explain the growth of some fibers and not others. It may be crucial that the lesion of axons descending from the brainstem occurs closer to the cell body than does that of the CST axons. Previous data suggest that cell body to axotomy distance does play a role in the axon growth potential of adult CNS neurons (Doster et al., 1991). It is also possible that different neuronal populations possess alternative myelin receptors, as discussed above. Perhaps the most plausible explanation for pathway-selective regeneration in *ngr*$^{-/-}$ mice is that NgR-independent inhibitory systems for Amino-Nogo and CSPG play a greater role in nonregenerating CST fibers. Further exploration of the basis of the differences between regeneration in different tracts should reveal additional determinants of CNS axonal regenerative capacity.

Behavioral Recovery

The regeneration of brainstem-spinal axons is correlated with improved recovery from spinal cord injury in the mice lacking NgR. Both electrophysiological and behavioral measurements reveal significantly greater improvement in the *ngr*$^{-/-}$ mice. The observation of significant recovery in control mice with low thoracic complete transection is consistent with previous studies (Leblond et al., 2003). It may reflect function based on either caudal intrinsic circuitry or a very small number of remaining fibers present in lateral uncut tissue bridges not recognized by GFAP immunohistology. Nonetheless, recovery is significantly improved in the *ngr*$^{-/-}$ mice, such that tcmMEP conduction and weight-bearing status are detected in a majority of these mice. There was no evidence of deleterious sprouting responses in the *ngr*$^{-/-}$ mice. Specifically, there was no increased evidence for neuropathic pain as exhibited by autophagia that might be caused by erroneous connectivity in motor pathways.

We observed regeneration of some serotonergic fibers in the absence of NgR. Furthermore, toxin studies demonstrate that 5HT fibers contribute significantly to recovery in the NgR null but not the control mice. Although there are reports on the detrimental effect of serotonergic transmission in the spinal cord in the acute phase of SCI, it has been previously recognized that distal serotonergic innervation is strongly correlated with locomotor recovery during the chronic phase (Antri et al., 2002; Saruhashi and Young, 1994; Saruhashi et al., 1996; Schmidt and Jordan, 2000). In fact, the threshold for locomotor recovery in a midthoracic lateral hemisection model in the rat was just 20% of normal 5-HT innervation (Saruhashi et al., 1996). Therefore, it is not surprising to find that despite modest levels of serotonergic sprouting in the distal cord of the knockouts, the level of locomotor improvement is considerably more prominent.

Comparison with Previous Nogo/NgR Studies

Both the selectivity of axon regeneration and the degree of behavioral improvement after dorsal spinal hemisection in *ngr*$^{-/-}$ mice can be compared with previous studies that perturb the Nogo system. The behavioral results here are not significantly different from those in anti-Nogo antibody-treated animals (Bregman et al., 1995), NEP1-40-treated animals (GrandPre et al., 2002; Li and Strittmatter, 2003), or NgRecto soluble protein-treated animals (S. Li, B.P.L., and S.M.S., unpublished data). Anatomically, the degree of raphespinal regeneration in this partial lesion seems quite similar in all of these cases. Since NgR and its ligands are common to these paradigms, they appear to account for the degree of recovery observed. One possible explanation for the lack of CST growth in the *ngr*$^{-/-}$ mice despite regeneration of other systems in these mice and despite the regeneration of the CST system in other studies is the role of Amino-Nogo. Selective Nogo-A upregulation might block CST regeneration in *ngr*$^{-/-}$ mice via enhanced Amino-Nogo action independently of NgR. In contrast, treatments with anti-Nogo antibody, NEP1-40, or NgRecto are acute and have not been shown to produce chronic compensatory alterations in gene expression of relevant molecules. Full consideration of an additional role of an Amino-Nogo receptor will require isolation of a receptor for that moiety and the development of specific means to perturb its function.

A comparison of *nogo*$^{-/-}$ and *ngr*$^{-/-}$ mice might be expected to be particularly informative about the match of ligand to receptor, and the role of Amino-Nogo versus Nogo-66 versus NgR. However, different strains of *nogo-a/b*$^{-/-}$ mice have been reported to exhibit either no CST axon regeneration (Zheng et al., 2003) or significant regeneration and functional recovery (Kim et al., 2003b). Selective *nogo-a*$^{-/-}$ mice are reported to exhibit a slight degree of CST sprouting after spinal cord section (Simonen et al., 2003). This in vivo discrepancy remains unexplained (Woolf, 2003), despite the fact that reduced myelin inhibition of axon growth in vitro is observed for both strains of *nogo-a/b*$^{-/-}$ mice (Kim et al., 2003b; Zheng et al., 2003). The variation between the ability of different fiber tracts to regenerate in *ngr*$^{-/-}$ mice demonstrates that both the Nogo/NgR system and other unidentified factors contribute to regulating the degree of axon growth. Such unidentified factors may play a role in explaining the phenotypic differences between different *nogo-a/b*$^{-/-}$ mice.

We have observed behavioral and electrophysiologic improvement after complete spinal transection only in the *ngr*$^{-/-}$ mice. Similar studies in the *nogo-a/b*$^{-/-}$ mice and with NEP1-40-treated rats did not reveal as great a level of improvement (data not shown). Therefore, the regenerative capacity of fiber systems descending from the brainstem to the spinal cord seems most dependent on NgR and its ligands, rather than on Amino-Nogo or other unidentified factors.

Astroglial Scar

While regeneration and recovery in the *ngr*$^{-/-}$ mice are greater than those in control mice, the total percentage

of regenerating fibers is much less than 100% even for those tracts that regenerate best, such as the raphespinal and rubrospinal tracts. The most likely explanation for the continued limitation to axon regeneration is inhibition from reactive gliosis. This hypothesis is based on previous work demonstrating the potent nature of these inhibitors in vivo and in vitro. It is striking that some fiber systems can negotiate regions of scar when relieved of NgR-dependent myelin inhibition. This raises the possibility that inhibition is to some extent cumulative along the axon and not expressed solely at the distal axon tip. In this way, relieving inhibition by myelin along the course of a descending axon might assist in its negotiation of scar components at the distal tip.

Behavioral Deficits in Uninjured Mice Lacking NgR

While mice lacking NgR exhibit generally good health and fertility, their behavior is altered from control mice in open field and rotarod testing. Specifically, the *ngr*$^{-/-}$ mice made fewer movements, avoided the center of the arena, and fell off of a spinning rod early. The anatomical and physiological basis for these changes is not clear. However, the presence of these deficits suggests that NgR contributes to the formation, refinement, or maintenance of some pathways required for normal mouse behavior. While NgR may be deleterious to mouse health by limiting regenerative responses after adult CNS trauma, it appears somewhat to be beneficial to complex animal behaviors prior to injury. Further studies, especially those utilizing conditional NgR gene targeting, will be required to separate these effects.

Experimental Procedures

Disruption of the *ngr* Gene by Homologous Recombination

Exon 2 of the mouse *ngr* gene was replaced with the *neo*^{R} cassette. After electroporation with the gene-targeting vector, ES cells (129/SvJ strain) were selected using G418 and FIAU. Chimeric mice were generated and crossed onto a C57BL/6J strain. Mice were backcrossed for another four to six generations and then intercrossed to yield homozygous knockouts. SCI experiments utilized littermate-matched female mice of different genotypes obtained from heterozygous × heterozygous or homozygous × heterozygous matings after four to six backcrosses to C57Bl6. Knockouts are born at normal Mendelian frequencies, and no unexpected deaths were observed.

Southern and Northern Analyses

For Southern blot analysis, tail DNA was extracted using the DNeasy Tissue Kit (Qiagen). Ten micrograms of DNA was digested with NheI, electrophoresed into an agarose gel, and blotted onto a nylon membrane. After UV crosslinking, the membrane was hybridized with PCR-generated random-primed ^{32}P-labeled *ngr* probes at 42°C in a 50% formamide/5× SSPE/10% dextran sulfate/1% SDS solution and washed at 62°C with 0.1× SSC/0.1% SDS. Routine genotypic screening was performed by PCR (*ngr*-specific forward primer, 5′-CAGTACCTGCGACTCAATGACAACCCC-3′; *ngr*-specific reverse primer, 5′-CTTCCGGGAACAACCTGGCCTCC-3′; *neo*^{R}-specific forward primer, 5′-CTATTCGGCTATGACTGGGCACAACAGAC-3′; *neo*^{R}-specific reverse primer, 5′-GAACTCGTCAAGAAGGCGATAGAAGG CGAT-3′).

For Northern blots, total brain RNA was isolated using the RNeasy Midi Kit (Qiagen). Total RNA (20 μg) was separated on a 1% agarose/2% formaldehyde/1× MOPS gel, blotted to a nylon membrane, UV crosslinked, and hybridized using ^{32}P-labeled probes prepared from fragments of *ngr* or *nogo-c* cDNA. Hybridization was performed at 65°C in 0.5 M phosphate buffer/1 mM EDTA/1% BSA/7% SDS, and washing was performed at 60°C with 0.2× SSC/0.5% SDS.

Immunoblotting

Brain was homogenized in RIPA buffer (1% Triton X-100/0.5% sodium deoxycholate/0.1% SDS/1× PBS) supplemented with 1× protease inhibitor cocktail mix (Roche) and sonicated, and the supernatant was collected after centrifugation. Brain lysate (20 μg) was separated by SDS-PAGE and blotted onto PVDF. Polyclonal rabbit anti-NgR antibodies were diluted 1:1000. Affinity-purified rabbit antibodies against Nogo-A were used at 50 ng/ml (Wang et al., 2002b). Rabbit anti-β-actin (Sigma) antibodies were diluted 1:1000. Goat polyclonal anti-MAG (R&D Systems) antibodies and mouse monoclonal anti-MBP (Sternberger Monoclonals) antibodies were diluted at 1:500 and 1:5000, respectively. Immunoreactivity was visualized after incubation with biotinylated secondary antibodies and avidin-AP (Vector Laboratories) using NBT/BCIP AP substrates. Densitometry of bands was carried out by scanning the blots into the computer and using NIH Image version 1.62 to determine the mean pixel density for each band.

AP-Nogo-66 Binding and Growth Cone Collapse Assays

P7-14 mouse DRG growth cone collapse and AP-Nogo-66 binding assays have been described (Fournier et al., 2001b; GrandPre et al., 2000). Briefly, plastic chamber slides were coated sequentially with 100 μg/ml poly-L-lysine and 10 μg/ml laminin before addition of DRG explants or dissociated DRG neurons. Explants were incubated for 48–72 hr before growth cone collapse was assessed in response to a 30 min exposure to various soluble ligands: IgG (Sigma), GST-Ng66-His (GrandPre et al., 2000), MAG-Fc (Liu et al., 2002; R&D Systems), OMgp (R&D Systems), and bovine CNS myelin (Fournier et al., 2001b; GrandPre et al., 2000). For binding assays, 50 nM AP-Nogo-66 or AP was incubated with dissociated neurons for 12 hr at 4°C prior to washing, fixation, heat inactivation, and staining for bound AP.

Behavioral Analysis

To assess open field activity, mice were acclimated for at least 30 min and then placed in the mouse activity monitoring cage (Columbus Instruments) for 15 min. Floor plane sensor measurements were collected using Opto-Max v.2.20-A software for a total of three sessions performed on three consecutive days. To assess locomotor coordination, mice were first trained on the rotarod (Columbus Instruments) for three sessions on two consecutive days. Performance on a speed setting with 0.1 rpm acceleration was recorded for three sessions on the third day.

Following SCI, a modified Basso-Beattie-Bresnahan (BBB) locomotor rating scale (Joshi and Fehlings, 2002) with 21 as normal and 0 as complete hindlimb paralysis was used to score locomotion in the open field after SCI (Basso et al., 1996). Another BBB modification that was developed to score mice as opposed to rats collapses values from 16 to 21 of the original rat scoring system to scores of 16 to 17 owing to the difficulties in making assessments at the upper end of the scoring range in mice (Dergham et al., 2002). Since all injured mice had BBB scores of 16 or less in the present study, this second mouse BBB scale modification is irrelevant to measurements of the injured mice in this study. Throughout the surgery, behavioral testing, and histological analysis, researchers were blind to the identity of the mouse genotype.

Spinal Cord Dorsal Hemisection, Complete Transection, Corticospinal and Rubrospinal Fiber Tracing, and 5,7-DHT Injection

All surgical procedures and postoperative care were performed in accordance with guidelines of the Yale Animal Care and Use Committee. Female mice (7–10 weeks old) were utilized for all SCI experiments, and in each case *ngr*$^{-/-}$ mice were compared with control *ngr*$^{+/-}$ and/or *ngr*$^{+/+}$ mice from the same litter (and therefore same strain background). Mice were deeply anesthetized with intraperitoneal ketamine (100 mg/kg) and xylazine (15 mg/kg). Laminectomies were performed at spinal levels T6 and T7, exposing the spinal cord. A dorsal hemisection was performed at T6 using the tip of a 32G needle, completely interrupting the dorsal and dorsolateral CSTs. For complete transections, laminectomies were performed at T8, and a no. 11 scalpel blade was used to transect the entire depth of the spinal cord. The vertebral cavity was probed several times with

fine forceps to ensure as complete a transection of the spinal cord and meninges as possible without disturbing the rostral or caudal spinal tissue (see Figure 6C). The muscle layers over the laminectomies were sutured, and the skin on the back was closed with surgical staples. For tracing the corticospinal tract, the scalp was cut, and a hole was drilled into the skull overlying the sensorimotor cortex. By four injections, 1.5 μl of the biotin dextran amine (BDA; MW 10,000; 10% in PBS; Molecular Probes) was applied. For tracing the rubrospinal tract, injections were performed bilaterally at the following coordinates: 2.5 mm posterior, 0.6 mm lateral to bregma, and 3.5 mm from the surface of the brain. BDA (200 nl) was injected over 3 min per side. Following injections, the scalp was closed with surgical staples. Ampicillin was administered intramuscularly twice daily for 3 days postoperatively, and the bladder was expressed by massage three times a day for the first postoperative week and then twice daily for the entire duration of survival.

For the mice receiving bilateral i.c.v. injections of the serotonin neurotoxin 5,7-dihydroxytryptamine (30 μg dissolved in 0.5 μl of 0.2% ascorbic acid in normal saline), the tip of a glass micropipette was positioned into the lateral cerebral ventricles (coordinates: 0.6 mm posterior to the bregma, 1.6 mm lateral from the sagittal suture, and 2 mm deep from the cortical surface) 4 weeks after complete transection. The duration of injection lasted for 2.5 min, and the micropipette was kept in position for an additional minute before withdrawal. Thirty minutes before the 5,7-DHT injection, the monoamine uptake inhibitor desipramine (25 mg/kg, i.p.; Sigma) was administered. Two weeks after 5,7-DHT injections, these mice were perfused for histological examination.

Histology and Analysis

Three weeks after dorsal hemisection or 6 weeks after complete transection, animals were perfused transcardially with PBS followed by a 4% paraformaldehyde/PBS solution. Spinal cords were dissected, postfixed overnight, and flash-frozen in tissue freezing medium (TBS) for cryostat sectioning. To visualize BDA-traced axons, 50 μm thick free-floating sections were preincubated with 0.5% BSA/0.1% Triton X-100/TBS and then processed with avidin-HRP (Elite ABC, Vector Laboratories) followed by a nickel-enhanced diaminobenzidine reaction. The sections were mounted, dehydrated, and coverslipped with DPX mounting medium (BDH Laboratory Supplies). For fiber counts, sections were examined with a 20× or 40× objective lens.

For immunohistochemistry, 50 μm thick free-floating sections of spinal cord were mounted and dried on glass slides and blocked in 3% normal goat serum/2% BSA/0.3% Triton X-100/PBS before incubation with polyclonal rabbit anti-5-HT (1:500; Immunostar). Polyclonal goat anti-5-HT antibodies (1:500; Immunostar) were used for double staining with rabbit anti-NgR antibodies (1:1000). Polyclonal rabbit anti-GFAP (Sigma) antibodies were diluted 1:50. The density of serotonin fiber innervation was determined using NIH Image version 1.62. Immunoreactive fibers were selected by thresholding, and then fiber length per spinal cord section was measured after utilizing the skeletonize function.

For camera lucida-style tracing of 5-HT-immunoreactive fibers and BDA-labeled rubrospinal fibers, serial longitudinal sections were digitally photographed, and fibers were traced on a computer using Adobe Photoshop 7.0 software.

Electrophysiological Recordings

To measure signal conduction in motor pathways after SCI, tcmMEPs were measured from mice 6 weeks after injury. To record the tcmMEP, mice were anesthetized with ketamine/xylazine i.p. Magnetic stimulation was delivered by positioning the center of a stimulator coil (MEP-10 magneto-electric stimulator set at 70% power with a 5 cm diameter coil; Cadwell Laboratories) over the cranium. The electromuscular response evoked by a 1.5 T magnetic discharge of 70 μs duration was recorded from either the gastrocnemius or biceps brachialis muscle. At least three replicate responses were recorded from each site. Lack of an evoked response after three trials for both hindlimbs was considered as having 0 μV tcmMEP amplitude.

Acknowledgments

We thank Marina Picciotto for assistance with mouse activity monitoring analysis. We thank Xiaofang Yang, Dike Qiu, Yiguang Fu, Stefano Sodi, and Ji Liao for expert technical assistance. This work was supported by grants to S.M.S. from the NIH and the McKnight Foundation for Neuroscience. J.H.P. is supported by an Institutional Medical Scientist Training Program grant from the N.I.H. S.M.S. is an Investigator of the Patrick and Catherine Weldon Donaghue Medical Research Foundation. Biogen Idec, Inc. partially supports this research and holds a license for NgR-related technology from Yale.

Received: January 23, 2004
Revised: August 30, 2004
Accepted: September 21, 2004
Published: October 27, 2004

References

Antri, M., Orsal, D., and Barthe, J.Y. (2002). Locomotor recovery in the chronic spinal rat: effects of long-term treatment with a 5-HT2 agonist. Eur. J. Neurosci. *16*, 467–476.

Barton, W.A., Liu, B.P., Tzvetkova, D., Jeffrey, P.D., Fournier, A.E., Sah, D., Cate, R., Strittmatter, S.M., and Nikolov, D.B. (2003). Structure and axon outgrowth inhibitor binding of the Nogo-66 receptor and related proteins. EMBO J. *22*, 3291–3302.

Bartsch, U., Bandtlow, C.E., Schnell, L., Bartsch, S., Spillmann, A.A., Rubin, B.P., Hillenbrand, R., Montag, D., Schwab, M.E., and Schachner, M. (1995). Lack of evidence that myelin-associated glycoprotein is a major inhibitor of axonal regeneration in the CNS. Neuron *15*, 1375–1381.

Basso, D.M., Beattie, M.S., and Bresnahan, J.C. (1996). Graded histological and locomotor outcomes after spinal cord contusion using the NYU weight-drop device versus transection. Exp. Neurol. *139*, 244–256.

Bonilla, I.E., Tanabe, K., and Strittmatter, S.M. (2002). Small proline-rich repeat protein 1A is expressed by axotomized neurons and promotes axonal outgrowth. J. Neurosci. *22*, 1303–1315.

Bregman, B.S., Kunkel-Bagden, E., Schnell, L., Dai, H.N., Gao, D., and Schwab, M.E. (1995). Recovery from spinal cord injury mediated by antibodies to neurite growth inhibitors. Nature *378*, 498–501.

Dergham, P., Ellezam, B., Essagian, C., Avedissian, H., Lubell, W.D., and McKerracher, L. (2002). Rho signaling pathway targeted to promote spinal cord repair. J. Neurosci. *22*, 6570–6577.

Domeniconi, M., Cao, Z., Spencer, T., Sivasankaran, R., Wang, K., Nikulina, E., Kimura, N., Cai, H., Deng, K., Gao, Y., et al. (2002). Myelin-associated glycoprotein interacts with the Nogo66 receptor to inhibit neurite outgrowth. Neuron *35*, 283–290.

Doster, S.K., Lozano, A.M., Aguayo, A.J., and Willard, M.B. (1991). Expression of the growth-associated protein GAP-43 in adult rat retinal ganglion cells following axon injury. Neuron *6*, 635–647.

Fournier, A.E., GrandPre, T., and Strittmatter, S.M. (2001a). Identification of a receptor mediating Nogo-66 inhibition of axonal regeneration. Nature *409*, 341–346.

Fournier, A.E., GrandPre, T., and Strittmatter, S.M. (2001b). Identification of a receptor mediating Nogo-66 inhibition of axonal regeneration. Nature *409*, 341–346.

GrandPre, T., Nakamura, F., Vartanian, T., and Strittmatter, S.M. (2000). Identification of the Nogo inhibitor of axon regeneration as a Reticulon protein. Nature *403*, 439–444.

GrandPre, T., Li, S., and Strittmatter, S.M. (2002). Nogo-66 receptor antagonist peptide promotes axonal regeneration. Nature *417*, 547–551.

Huber, A.B., Weinmann, O., Brosamle, C., Oertle, T., and Schwab, M.E. (2002). Patterns of nogo mRNA and protein expression in the developing and adult rat and after CNS lesions. J. Neurosci. *22*, 3553–3567.

Joshi, M., and Fehlings, M.G. (2002). Development and characterization of a novel, graded model of clip compressive spinal cord injury

in the mouse: Part 1. Clip design, behavioral outcomes, and histopathology. J. Neurotrauma *19*, 175–190.

Kim, J.E., Bonilla, I.E., Qiu, D., and Strittmatter, S.M. (2003a). Nogo-C is sufficient to delay nerve regeneration. Mol. Cell. Neurosci. *23*, 451–459.

Kim, J.E., Li, S., GrandPre, T., Qiu, D., and Strittmatter, S.M. (2003b). Axon regeneration in young adult mice lacking Nogo-A/B. Neuron *38*, 187–199.

Lauren, J., Airaksinen, M.S., Saarma, M., and Timmusk, T. (2003). Two novel mammalian Nogo receptor homologs differentially expressed in the central and peripheral nervous systems. Mol. Cell. Neurosci. *24*, 581–594.

Leblond, H., L'Esperance, M., Orsal, D., and Rossignol, S. (2003). Treadmill locomotion in the intact and spinal mouse. J. Neurosci. *23*, 11411–11419.

Li, S., and Strittmatter, S.M. (2003). Delayed systemic Nogo-66 receptor antagonist promotes recovery from spinal cord injury. J. Neurosci. *23*, 4219–4227.

Liu, B.P., Fournier, A., GrandPre, T., and Strittmatter, S.M. (2002). Myelin-associated glycoprotein as a functional ligand for the Nogo-66 receptor. Science *297*, 1190–1193.

McGee, A.W., and Strittmatter, S.M. (2003). The Nogo-66 receptor: focusing myelin inhibition of axon regeneration. Trends Neurosci. *26*, 193–198.

Saruhashi, Y., and Young, W. (1994). Effect of mianserin on locomotory function after thoracic spinal cord hemisection in rats. Exp. Neurol. *129*, 207–216.

Saruhashi, Y., Young, W., and Perkins, R. (1996). The recovery of 5-HT immunoreactivity in lumbosacral spinal cord and locomotor function after thoracic hemisection. Exp. Neurol. *139*, 203–213.

Schmidt, B.J., and Jordan, L.M. (2000). The role of serotonin in reflex modulation and locomotor rhythm production in the mammalian spinal cord. Brain Res. Bull. *53*, 689–710.

Simonen, M., Pedersen, V., Weinmann, O., Schnell, L., Buss, A., Ledermann, B., Christ, F., Sansig, G., van der Putten, H., and Schwab, M.E. (2003). Systemic deletion of the myelin-associated outgrowth inhibitor Nogo-A improves regenerative and plastic responses after spinal cord injury. Neuron *38*, 201–211.

Wang, K.C., Koprivica, V., Kim, J.A., Sivasankaran, R., Guo, Y., Neve, R.L., and He, Z. (2002a). Oligodendrocyte-myelin glycoprotein is a Nogo receptor ligand that inhibits neurite outgrowth. Nature *417*, 941–944.

Wang, X., Chun, S.J., Treloar, H., Vartanian, T., Greer, C.A., and Strittmatter, S.M. (2002b). Localization of Nogo-A and Nogo-66 receptor proteins at sites of axon-myelin and synaptic contact. J. Neurosci. *22*, 5505–5515.

Woolf, C.J. (2003). No Nogo: now where to go? Neuron *38*, 153–156.

Zheng, B., Ho, C., Li, S., Keirstead, H., Steward, O., and Tessier-Lavigne, M. (2003). Lack of enhanced spinal regeneration in Nogo-deficient mice. Neuron *38*, 213–224.